Draft version April 15, 2015
Preprint typeset using LaTeX style emulateapj v. 5/2/11

arXiv:1410.7422v2 [astro-ph.IM] 14 Apr 2015

PULSAR OBSERVATIONS USING THE FIRST STATION OF THE LONG WAVELENGTH ARRAY AND THE LWA PULSAR DATA ARCHIVE

K. Stovall[1], P. S. Ray[2], J. Blythe[2], J. Dowell[1], T. Eftekhari[1], A. Garcia[3], T. J. W. Lazio[4], M. McCrackan[1], F. K. Schinzel[1], G. B. Taylor[1]

Draft version April 15, 2015

ABSTRACT

We present initial pulsar results from the first station of the Long Wavelength Array (LWA1) obtained during the commissioning period of LWA1 and early science results. We present detections of periodic emission from 44 previously known pulsars, including 3 millisecond pulsars (MSPs). The effects of the interstellar medium on pulsar emission are significantly enhanced at the low frequencies of the LWA1 band (10–88 MHz), making LWA1 a very sensitive instrument for characterizing changes in dispersion measures (DM) and other effects from the interstellar medium. Pulsars also often have significant evolution in their pulse profile at low frequency and a break in their spectral index. We report DM measurements for 44 pulsars, mean flux density measurements for 36 pulsars, and multi-frequency component spacing and widths for 15 pulsars with more than one profile component. For 27 pulsars, we report spectral index measurements within our frequency range. We also introduce the LWA1 Pulsar Data Archive, which stores reduced data products from LWA1 pulsar observations. Reduced data products for the observations presented here can be found on the archive. Reduced data products from future LWA1 pulsar observations will also be made available through the archive.

Subject headings: pulsars: general

1. INTRODUCTION

Though pulsars were originally discovered at 81.5 MHz (Hewish et al. 1968) and much of the initial follow-up of them were conducted at low frequencies (below 200 MHz), the majority of pulsar observations conducted after the mid-1970s moved to frequencies of about 350 MHz and above. This move to higher frequencies was largely due to three reasons. The first is the detectability of pulsars due to radio wave propagation effects through the interstellar medium (ISM), in particular dispersion and scattering. The time delay as a function of frequency (ν) due to the dispersive properties of the ISM scales as ν^{-2}. Though this effect is largely correctable through the use of incoherent dedispersive techniques and completely correctable using coherent dedispersive techniques, these techniques require large computational resources and have only recently begun to be viable for regular use in low frequency observations. The effects of interstellar scattering broaden a pulse roughly as ν^{-4}. These effects are not correctable without a clear detection of a scattered pulse and therefore a pulse which is completely scattered out cannot be recovered. The second reason which led to the majority of pulsar observations being conducted at higher frequencies is that many pulsars have an intrinsic spectral turnover at around 100-200 MHz. Therefore, observations at higher frequencies often result in higher quality detections. A third reason pulsar observations moved to higher frequency is the large sky temperature from Galactic synchrotron emission. Pulsars are generally steep spectrum sources with typical spectral indices for their flux densities of about -1.4 (Bates et al. 2013). However, the Galactic background is also bright at low frequencies and has a brightness temperature spectral index of -2.6 (Haslam et al. 1982).

1.1. *Low Frequency Profile Evolution and Spectral Turnover*

Despite the previously described difficulties in observing pulsars at low frequencies, such observations are necessary to fully understand the pulsar emission mechanism. Many effects that are intrinsic to the pulsar are observed, such as intrinsic profile evolution and a spectral turnover in a large fraction of pulsars. A typical form of intrinsic profile evolution is the so-called "radius-to-frequency" (RFM) mapping effect, which postulates that lower frequencies are emitted higher in the pulsar's magnetosphere, resulting in wider pulse profiles at low frequency than at high frequency (Cordes 1978). Observationally, RFM is most prominent at the lowest frequencies and may only be exhibited below about 1 GHz (Thorsett 1991). In Rankin (1983) and other papers in a series on the pulsar emission mechanism, the authors modeled pulsar emission as 'core' emission coming from near the magnetic pole and 'cone' emission from a number of concentric cones. The authors noted that 'core' emission tends to have a steeper spectral index versus that of 'cone' emission and theorized that the two may even be the result of different emission mechanisms. Another model put forward by Lyne & Manchester (1988) explains the emission from pulsars as randomly located patches of emission within a 'window function.' Other models which combine aspects of the above two models have also been suggested. For example, Karastergiou & Johnston (2007) postulated that

[1] Department of Physics and Astronomy, University of New Mexico, Albuquerque, NM, USA; stovall.kevin@gmail.com
[2] Space Science Division, Naval Research Laboratory, Washington, DC 20375-5352, USA
[3] Center for Advanced Radio Astronomy, University of Texas at Brownsville, One West University Boulevard, Brownsville, Texas 78520, USA
[4] Jet Propulsion Laboratory, California Institute of Technology, 4800 Oak Grove Drive, Pasadena, CA, 91106, USA

patchy emission for a particular frequency could originate at varying heights within the pulsar's magnetosphere. In this model, the 'core' emission is coming from closer to the neutron star's surface while the 'cone' emission comes from higher in the magnetosphere. Measurements of profile evolution for a wide range of frequencies for a large population of pulsars are necessary to constrain these theories.

At frequencies above a few hundred MHz, the pulsar spectrum is typically modeled as a power law of the form $S_\nu \propto \nu^{-\alpha}$, where typical values for α are around -1.4 (Bates et al. 2013). However, many pulsars exhibit a low frequency turnover in their spectrum in the 100-200 MHz range (see for example, Malofeev et al. 1994), others have a spectral turnover at higher ($\sim$1 GHz) frequencies (e.g. Kijak et al. 2007; Dembska et al. 2014), and still others have not shown a turnover at any frequency at which they have been detected (Malofeev et al. 1994). Development of a complete theory for the pulsar emission mechanism must account for the observed profile evolution described above and these spectral properties, therefore further characterization of these effects in a large number of pulsars is warranted.

1.2. *Dispersion and Scattering by the ISM*

For an overview of the effects of the ISM on pulsar signals, see Cordes (2002). Two of the ISM effects are dispersion and scattering, whose effects follow ν^{-2} and ν^{-4} dependencies, respectively. Due to these dependencies, these effects are significantly stronger and can be very precisely measured at lower frequencies and, therefore measurements of the dispersion measure (DM) and scattering can be used to monitor the characteristics of the ISM along the lines-of-sight to pulsars. Such precise measurements enable the testing of the cold plasma dispersion model (Phillips 1991) and deviations from the ν^{-4} dependence of pulse broadening (Löhmer et al. 2001).

Another potential application of these precise measurements are to correct for time dependent dispersion and scattering changes in high precision pulsar timing such as is done in pulsar timing array (PTA) experiments attempting to detect low frequency gravitational wave emission (van Haasteren et al. 2011; Manchester et al. 2012; Demorest et al. 2013). The efforts to detect gravitational waves (GWs) using PTAs are greatly constrained by the ability to understand and mitigate various sources of noise in the MSP timing residuals. Important sources of noise in the timing residuals are DM variations in time and frequency and pulse broadening due to scattering (Cordes & Shannon 2010). It is currently unclear whether or not observations of DM and scattering effects at low frequencies can be used to directly correct PTA datasets. Simulations suggest that measurements of DM variations at low frequencies are unlikely to be useful in direct correction for DM variation (Cordes et al. 2015). However, such observations will at the very least provide a better understanding of the ISM and could prove to at least partially correct for these variations.

1.3. *New Low Frequency Facilities*

In recent years, many low-frequency observatories have come on line, including the first station of the Long Wavelength Array (LWA1; described in more detail below, but also see Taylor et al. 2012), the Low Frequency Array (LOFAR; van Haarlem et al. 2013; Stappers et al. 2011), and the Murchison Widefield Array (MWA; Tingay et al. 2013; Tremblay et al. 2015). The development of these systems is largely due to interest in detecting the epoch of re-ionization. While the detection of signatures from the epoch of reionization was a key requirements driver for LOFAR and MWA, LWA1 originated with the goal of creating a multi-purpose instrument operating in a relatively unexplored region of the radio spectrum. Another low frequency instrument, the Ukrainian T-shaped Radio telescope, second modification (UTR-2; Braude et al. 1978) has recently received an upgraded backend system (Ryabov et al. 2010), making it significantly more sensitive to radio pulsar emission (Zakharenko et al. 2013). With these new systems beginning to come on line and with computational resources now capable of mitigating the effects of dispersive smearing, observations of pulsars at frequencies below about 200 MHz are beginning to be performed more regularly. Pulsar detections for 40 pulsars at about 20 MHz using UTR-2 were reported in Zakharenko et al. (2013), 100 pulsars at about 150 MHz as well as 27 pulsars at 40 MHz have been reported in Pilia et al. (2015), and this work reports on detections of 44 pulsars in the 30 to 88 MHz range. In addition to detections from a large number of pulsars, studies of individual pulsars have also begun to be performed. Examples include observations of MSPs with LWA1 and the MWA (Dowell et al. 2013; Bhat et al. 2014), observations of the mode-switching PSR B0943+10 (Bilous et al. 2014), and a study of the effects of profile evolution on measured DMs (Hassall et al. 2012).

In this paper, we present pulsar observations made with LWA1 and introduce the LWA Pulsar Data Archive. In Section 2, we will describe LWA1. In Section 3, we will present how LWA1 pulsar data has been processed. In Section 4, we will introduce the LWA1 Pulsar Data Archive and how to access pulsar data from previous observations. In Section 5 we will describe the methods we used to measure the DM and mean flux density. In Section 6, we will detail current observations of known pulsars using LWA1.

2. THE FIRST STATION OF THE LONG WAVELENGTH ARRAY

Here we briefly describe LWA1 as relevant to pulsar observations, for a detailed, general description of LWA1 see Taylor et al. (2012) and Ellingson et al. (2013b). LWA1 is capable of tracking four sky locations using independent delay-and-sum beams. These beams each have two independent frequency ranges called tunings, each with dual polarization. These tunings can have a center frequency in the range of 10-88 MHz and have a frequency tagging better than 1 mHz (Schinzel & Dowell 2014). The LWA1 data are timetagged by the digital processor using a system clock-based counter that is synchronized with the station's GPS receiver. The GPS receiver provides both the absolute time, as well as the signals needed to generate the system clock: a 1 pulse per second and a 10 MHz signal. The 10 MHz signal is generated using an internal rubidium oscillator that provides an accuracy better than one part in 10^{11} when

the GPS receiver is locked. LWA1 can be operated in full-bandwidth mode which does not filter any of the 10-88 MHz frequency range, or in split-bandwidth, which attenuates signals received below about 30 MHz. A majority of pulsar observations have been taken in split-bandwidth mode in order to mitigate the effects of RFI at frequencies below about 25 MHz. Typically, pulsar observations are recorded in baseband mode at a sample rate of 19.6 megasamples per second. Since the samples are complex, this allows a bandwidth up to 19.6 MHz (17-18 MHz usable). In cases where the data rate for this mode is too large and the desired science can be accomplished with less bandwidth, data can be recorded using lower sample rates. Results presented here (except where otherwise noted) were taken in split bandwidth mode with the full 19.6 MHz of bandwidth in baseband mode and then were converted into a filterbank with 4,096 channels and a sample time of 209 μs using tools described in Sec. 3 and Dowell et al. (2012).

The RFI environment of LWA1 varies with time of day and observing frequency. RFI is generally stronger during the day, especially at the lower part of the LWA1 band (below about 25 MHz). LWA1 was designed to operate between where the Earth's Ionosphere becomes transparent to radio waves at about 10 MHz up to the lower part of the FM band at 88 MHz. There are some strong frequency carriers within the LWA1 band (for example, analog TV channel 2 at 55.25 MHz), but most of the band is generally clean. Other sources of terrestrial RFI in the LWA1 band are CB and HF radio transmissions, but they are intermittent and dependent on the state of the ionosphere and therefore are not a problem much of the time. Pulsar observations presented in Section 6 were processed using a RFI mask that we calculated using the `rfifind` tool from the Pulsar Search and Exploration Toolkit[5] (`PRESTO`; Ransom 2001) pulsar reduction package. Table 2 gives the fraction of observations with percentages of data masked below 5%, 10%, 25%, and 50% for various frequencies and times of day. Frequencies near the edge of the LWA1 band are more affected by RFI than the middle section of the band. Since most of our observations were done above 30 MHz, we do not see much variation in RFI as a function of time of day, though the cleanest time is from 0 to 4 hours local time.

3. LWA1 PULSAR DATA PROCESSING

A set of software tools available for processing data from LWA1 are available in the LWA Software Library[6] (LSL; Dowell et al. 2012). A number of tools useful for processing pulsar data are included in the 'Pulsar' extension to LSL. A majority of pulsar observations are processed with `writePsrfits2.py`, a tool that synthesizes a filterbank from the raw beam data and stores the results in PSRFITS (Hotan et al. 2004) format. The data can then be further processed using typical pulsar data reduction methods.

Due to the extreme effects of dispersion at LWA1 frequencies, many pulsars require coherent dedispersion be applied in order to avoid smearing of the pulses within a frequency channel. For these pulsars, the `writePsrfits2D.py` can be used. This tool is similar to `writePsrfits2.py`, but coherent de-dispersion is applied on a per-channel basis after the filterbank. The de-dispersion method is an optimized C-based implementation of the de-dispersion module available in LSL. The C-based code uses both OpenMP to parallelize the process across channels and the FFTW library (Frigo & Johnson 1998) for optimized Fourier transforms. The placement of the de-dispersion after the filterbank allows for this process to be more memory efficient since the dispersion delay within a single channel is less than the sub-integration block size.

Though the maximum bandwidth of a single tuning is 19.6 MHz, if the center frequency of the tunings are chosen with appropriate spacing, they can be combined into a single data file. This includes tunings recorded with a separate beam, though in this case, the PSRFITS file must be created using `writePsrfits2Multi.py` or `writePsrfits2DMulti.py`, which are tools that aligns the start and end point for files taken simultaneously using different LWA beams. Figure 1 shows a plot of PSR B1919+21 taken with two beams with tuning center frequencies of 35.1, 49.8, 64.5, and 79.2 MHz, each at 19.6 MHz bandwidth. The data were processed using `writePsrfits2Multi.py` and then combined in frequency.

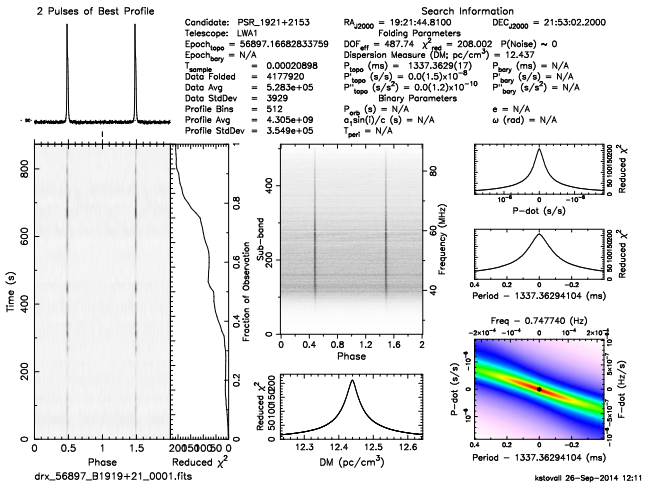

Figure 1. PRESTO diagnostic plot of a 15 minute integration on PSR B1919+21 covering the entire split-bandwidth configuration of LWA1 using 2 LWA1 beams, that has been combined using `LSL`'s `writePsrfits2Multi.py` tool.

4. LWA PULSAR DATA ARCHIVE

We have begun to store reduced data products from pulsar observations and have made them publicly available on the LWA Pulsar Data Archive[7]. These data products can be used for the generation of pulse times-of-arrival (TOAs), analysis of single pulse properties, and analysis of the pulse profile for each pulsar detection that has been made. Much of the data used in this paper and that are now available on the archive are the result of commissioning efforts and early pulsar project observations, however since LWA1 is now operating as

[5] http://www.cv.nrao.edu/~sransom/presto/

[6] `http://fornax.phys.unm.edu/lwa/trac/wiki`

[7] `http://lda10g.alliance.unm.edu/PulsarArchive/`

Freq (MHz)	N	<5%	<10%	<25%	<50%	Hour (local time)	N	<5%	<10%	<25%	<50%
30 - 40	68	0.68	0.78	0.84	0.93	00 - 04	42	0.79	0.93	1.00	1.00
40 - 50	64	0.78	0.89	0.98	1.00	04 - 08	54	0.76	0.93	0.94	0.98
50 - 60	44	0.84	0.91	1.00	1.00	08 - 12	23	0.78	0.78	0.91	0.96
60 - 70	69	0.86	0.90	0.97	0.99	12 - 16	61	0.72	0.82	0.90	0.95
70 - 80	94	0.64	0.86	0.95	0.96	16 - 20	78	0.76	0.94	0.97	0.99
						20 - 24	99	0.68	0.76	0.91	0.94

Table 1
Left: Fraction of datasets within various frequency ranges with percentages of data masked below 5%, 10%, 25%, and 50%. Right: Fraction of datasets with percentages of data masked below 5%, 10%, 25%, and 50% as a function of local time.

an University Radio Observatory and telescope time allocation is awarded through a proposal system, projects which have been awarded time have a 1-year proprietary period for their data. Following the proprietary period, reduced data products from pulsar observations will be made available through the archive. The data products from each observation include the folded result from `PRESTO`), folded results in PSRFITS format, folded results from `DSPSR`[8], a search format file with the data sub-banded using the LWA1 determined DM into 128 frequency channels, a timeseries which has been de-dispersed at the LWA1 determined DM, a timeseries at DM=0 pc cm^{-3}, and RFI masking information. We provide a more detailed description of the available reduced products below.

- The `PRESTO` folded results include two folded products; one which uses the best known ephemeris for the pulsar and another which starts with the best known ephemeris but searches for the optimal period, period derivative, and DM for the observation. The results include the folded data, an image of the folded result in postscript and png formats, and an ASCII text file containing the best profile for that observation. These results are appropriate for pulse profile analysis and generation of pulsar TOAs.

- Folded results in PSRFITS format (made using `fold_psrfits` and DSPSR) are generated to allow the use of various tools from `PSRCHIVE`[9] to analyze the observation. The data consists of 2048 bins across the profile with 60-s subintegrations, using the full frequency resolution of the original data file. The folded profiles generated using DSPSR are typically made with full Stokes parameters, while the ones generated using `fold_psrfits` contain only total intensity.

- The sub-banded data reduces the number of frequency channels to 128 (typically from 4096) by de-dispersing at the LWA1 determined DM and then summing channels. This data preserves the individual pulses as well as the original time resolution. The data can be used for generating additional folded results or for analysis of single pulse characteristics.

- The individual de-dispersed timeseries loses all of the original frequency information, but preserves the original time resolution. It can be used for quick folding of data and analysis of individual pulses.

- The zero-DM timeseries is included so that the RFI environment is known for singlepulse studies as well as to provide additional information on the general RFI environment of LWA1.

- RFI mask information, obtained using `PRESTO`'s `rfifind` program, has been included to inform data users of the RFI environment for their particular observation and to provide a long term record of the LWA1 RFI. Typically, the mask information is obtained by analyzing 10 second long pieces, however this can vary based on the parameters of the observation.

[8] http://dspsr.sourceforge.net/
[9] http://psrchive.sourceforge.net/

5. DM, MEAN FLUX DENSITY, AND PULSE COMPONENT ANALYSIS

For the pulsars that we have detected, we immediately obtain a measurement of their DM and we have estimated their flux density. For some pulsars, the emission shows the distinct signature of having been scattered by the interstellar medium, but we leave the measurement of scatter broadening to a future study.

5.1. *DM*

The measured DM for a pulsar can be time variable, due to motion of the pulsar relative to the Earth and a changing ISM (for example; Phillips & Wolszczan 1991). These changes can be stochastic or can have a trend over time. Typically, the DM variations are of the order of 10^{-3} to 10^{-2} pc cm^{-3} yr^{-1}. Profile evolution and interstellar scattering can cause systematic errors in the measurement of the absolute DM of a pulsar. The pulse profile of a pulsar often evolves with frequency and, therefore, it is not always clear how to properly align template profiles at different frequencies. In Ahuja et al. (2007), the authors showed through simulation of profile evolution that the true DM can significantly be affected, particularly for pulsars with complex, asymmetric profiles. Hassall et al. (2012) showed using real pulsar data that this DM error could be corrected by finding a fiducial point in the profile and modeling the pulse profile as a function of frequency. Interstellar scattering is also a frequency dependent effect which causes the centroid of a pulse to be delayed at lower frequencies and can bias the measurement of DM. As a starting point, we used a simplified approach based on single templates (described in more detail below) and leave the more complex modeling of interstellar scattering and frequency evolution to future work. Due to our more simplified approach, pulsars

with complex profile evolution and interstellar scattering have a bias in their DM measurement, however the error in these DM measurements are still indicative of the precision with which DMs can be determined with LWA1.

For all of the pulsars that we detected, we obtained a measurement of the DM using the following method. For slow pulsars, we folded each of the observations using ephemerides from the ATNF pulsar catalog. The MSPs were folded using ephemerides from Demorest (2015) for PSRs J0030+0451 and J2145−0750 and Desvignes, G. (2015) for PSR J0034−0534. We then generated a standard template profile, typically using observations around 50-60 MHz. We then obtained TOAs across the frequency band (typically 4 TOAs per tuning). These TOAs were calculated by doing a least squares fit in the Fourier domain (Taylor 1992). We then used `TEMPO`[10] to fit these TOAs for the best DM for the observation, leaving all other parameters fixed. The size of errors for our measured DM calculated this way depends on the pulse width and shape as well as the SNR of the pulsar detection, however typical 1-sigma error values range from about 10^{-2} pc cm^{-3} for weak, slow pulsars to 5×10^{-5} pc cm^{-3} for millisecond pulsars. Figure 2 shows a plot of the DM for PSR J2145-0750 calculated using the above method for 8 epochs.

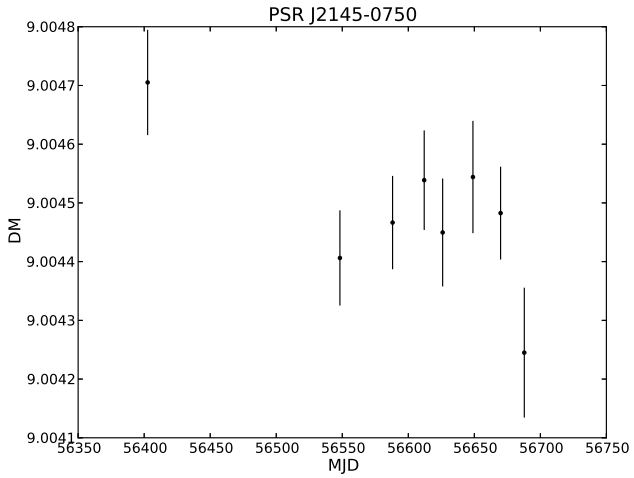

Figure 2. The DM of PSR J2145-0750 as measured by LWA1 at 8 different epochs.

5.2. *Mean Flux Density*

The system equivalent flux density (SEFD) of LWA1 varies with observing frequency, zenith angle, and local sidereal time (LST). In Schinzel & Polisensky (2014) the authors observed the bright known radio sources, Cyg A, Cas A, Tau A, Vir A, at varying zenith angles and frequencies. We used the results from this observing program to estimate the response of LWA1 to varying zenith angle, and used each source to determine the SEFD for Stokes' I at zenith. The SEFD was determined following the drift scan method described in Ellingson et al. (2013b). The derived SEFDs for each object were then converted to a SEFD at zenith by applying an empirically derived power ratio correction with respect to zenith for Stokes' I:

$$\mathrm{SEFD(zenith)} = \mathrm{SEFD(obs)} / \left(166.625 * E^{-1.251} + 0.401\right), \quad (1)$$

where E is the elevation of the observed object in degrees. After this the zenith SEFD values were averaged per frequency bin. We found that the resulting SEFD is fairly constant across our observing band, but increases below 40 MHz. We then used the combined measurement of the SEFD at zenith and the fitted zenith angle dependence to estimate the SEFD for each of our pulsar observations. The error in the measurement of LWA1's zenith angle SEFD is about 25%, but to account for errors caused by SEFD variation with LST (which we are not accounting for in this work) and error in the fit of the function to zenith angle dependence, we use a total error of 50%.

The results from Schinzel & Polisensky (2014) are only applicable for observations from LWA1 since the last calibration of the LWA1 cable delays, which occurred on 2013 Feb 28, so we have limited our mean flux density estimates to observations that occurred after this date. For each observation, we calculated the appropriate SEFD as described above and used the radiometer equation (Dewey et al. 1985) to estimate the mean flux density. For pulsars with mean flux density measurements at 3 or more frequencies, we then assumed a power law of the form $S_\nu \propto \nu^\alpha$ and performed a least squares fit to our measured mean flux densities.

5.3. *Pulse Component Analysis*

During the Gaussian fitting process, 15 pulsars clearly required multiple Gaussian components, ignoring pulsars that showed the effects of interstellar scattering. There are 10 and 5 pulsars requiring 2 components and 3 components, respectively. None of the profiles required more than 3 components. For these multi-component pulsars, we performed Gaussian fits at each frequency for which we have data in hand and calculated the widths of each component as a function of frequency as well as the relative spacing of the components. During this analysis we ordered the components based on their pulse phase, so that component 1 occurs earliest in the profile. Using the terminology of Rankin (1983), the 3-component profiles have conal emission labeled as components 1 and 3, while the bridge or core emission is labeled component 2. At some frequencies for PSR B0950+08, the phase of the core emission was slightly smaller than the leading edge of the conal emission. We kept the same component labels and the component spacing for these cases have a negative sign. For the pulsars with 2 components, we then compared the relative amplitudes of the fitted Gaussians by calculating the ratio of the two components $A_{21} = \frac{A_2}{A_1}$ where A_1 is the amplitude of the first component (smaller pulse phase) and A_2 is the second component (larger pulse phase).

6. OBSERVATIONS & RESULTS

Here we present initial pulsar results using LWA1. The majority of data presented here were taken throughout commissioning activities and during early science runs. In some cases, pulsars were used to verify data integrity

[10] `http://tempo.sourceforge.net`

for other science targets. Therefore, they were taken in a variety of observing modes, over a wide range of dates (2012 May 11 to 2015 March 1), and were not processed in a uniform way. As of 2015 March 1, LWA1 has been used to detect periodic emission from 44 pulsars and giant bursts from another (B0531+21; Ellingson et al. 2013a). Large individual pulses have also been reported from PSR B0950+08 (Tsai et al. 2015), which is one of the sources for which we report periodic emission. We present profiles at various frequencies for 44 pulsars in Fig. 3. Due to the differences in data reduction and time difference between observations, the cause of profile offsets from one frequency to another is not clear. Therefore, for the majority of profiles, we aligned them manually by shifting the peak of each profile to the middle. However, PSRs B0031-07, B0320+39, and B0809+74 show considerable profile evolution as a function of frequency throughout the LWA1 frequency band, so these profiles were aligned "by eye". Though we leave out an analysis of scattering due to the ISM, the profile evolution across the LWA1 band for 10 pulsars (PSRs B0329+54, B0450+55, B0823+26, B0919+06, B1508+55, B1541+09, B1822-09, B1839+56, B1842+14, and B2217+47) show evidence of scattering. We have also detected the mode switching PSR B0943+10 (Suleymanova & Izvekova 1984; Bilous et al. 2014) in both bright (B) and quiet (Q) mode and the resulting profiles are shown in Figure 3.

6.1. *DM*

Table 6.2 contains a list of 44 previously known pulsars detected through periodicity, the pulsar's period and DM as reported by the ATNF, and our DM measurement determined as described in Section 5.1. The two rightmost columns show DM values reported by (Zakharenko et al. 2013). The largest difference in DM between the ATNF and LWA1 results occurred for PSR B0031-07, but the change of 0.016 pc cm^{-3} yr^{-1} is comparable in magnitude to previously observed DM variation. However, as noted in Section 5.1, pulsars with asymmetric profiles can have a bias in their DM due to profile evolution. PSR B0031-07 is seen to have substantial profile evolution in our observations, so this DM bias could account for part of the DM difference. Further analysis of DM variations with time will be presented for a sub-sample of pulsars (including the 3 MSPs J0030+0451, J0034-0534, and J2145-0750) in a future paper.

6.2. *Mean Flux Density*

We present mean flux densities determined as described in Section 5.2 as well as the full width at half maximum (w_{50}) and full width at 10% of maximum (w_{10}) for 36 pulsars in Table 3. We did not measure flux densities for 8 of the pulsars detected with LWA1, due to only having observations from before 2013 Feb 28, the date of the last cable delay calibration. In Figure 4, we show our flux density measurements with other reported values at comparable frequencies (Sieber 1973; Izvekova et al. 1979, 1981; Shrauner et al. 1998; Karuppusamy et al. 2011; Zakharenko et al. 2013; Lane et al. 2014). We have included higher frequency measurements from Sieber (1973) to show the general behavior of the spectrum of each of these pulsars at higher frequency. Most of our measurements are in agreement with past values, allowing for slight variability in flux and for scintillation. Our measurements indicate larger values for PSRs B0031-07, B0329+54, and B1133+16 than previous measurements. Since our measurements of flux density are from a single epoch, additional measurements are needed to determine whether these discrepancies are due to these pulsars being brighter due to favorable scintillation (possibly due to ISM or Ionospheric activity) or whether it is a systematic effect either of LWA1 or from our SEFD estimation method. We expect that we will be able to reduce the size of the error on mean flux measurements in the future by adding additional parameters, such as variation with LST, to the SEFD determination procedure described in 5.2. Even with the increased flux measurements in the 3 pulsars mentioned above, a general trend of spectral turnover is observed in the spectra in Figure 4.

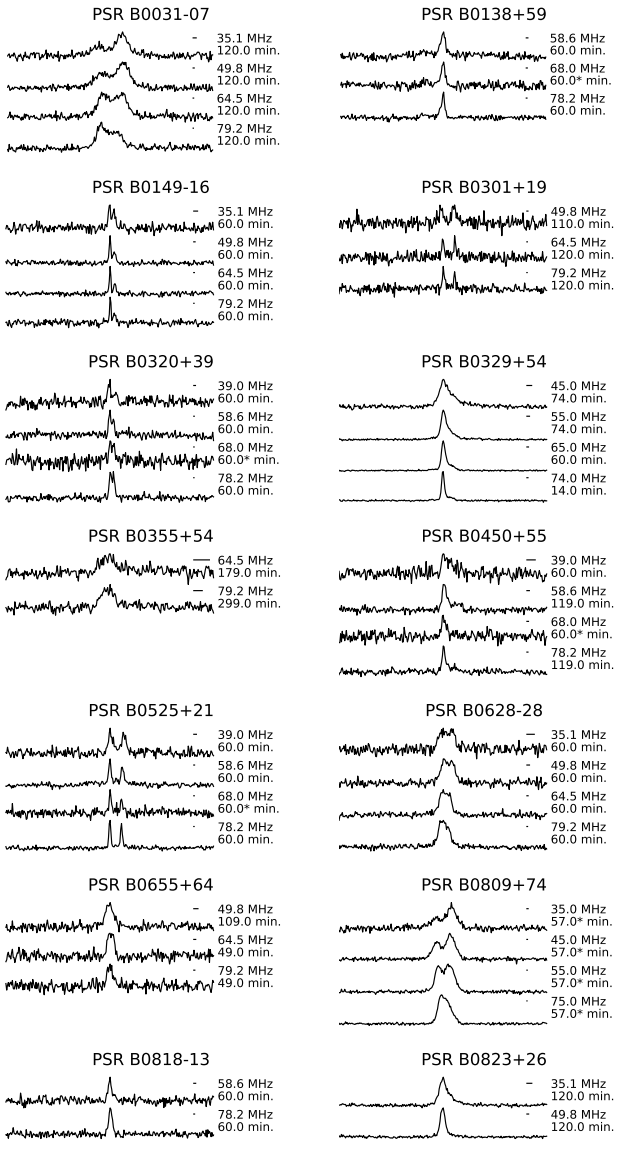

Pulsar	P	DM_{ATNF}	DM^{ATNF}_{Epoch}	DM_{LWA1}	DM^{LWA1}_{Epoch}	DM_{UTR2}	DM^{UTR2}_{Epoch}
	s	pc cm^{-3}		pc cm^{-3}		pc cm^{-3}	
J0030+0451	0.0049	4.333(1)	50984	4.33252(4)	56560		
B0031-07	0.9430	11.38(8)	46635	10.922(6)	56843	10.896(4)	55480
J0034-0534	0.0019	13.76517(4)	50690	13.76505(4)	56631		
B0138+59	1.2229	34.797(11)	49293	34.926(4)	56563		
B0149-16	0.8327	11.922(4)	48227	11.92577(4)	56955		
B0301+19	1.3876	15.737(9)	49289	15.68(3)	57035		
B0320+39	3.0321	26.01(3)	49290	26.173(2)	56563	26.162(11)	55480
B0329+54	0.7145	26.7641(1)	46473	26.779(1)	56364	25.661(11)	55480
B0355+54	0.1564	57.1420(3)	49616	57.1453(8)	56674		
B0450+55	0.3407	14.495(7)	49910	14.5943(9)	56564	14.602(5)	55480
B0525+21	3.7455	50.937(17)	54200	50.93(1)	56565		
B0628-28	1.2444	34.468(17)	46603	34.425(1)	56706		
B0655+64	0.1957	8.771(5)	48806	8.777(1)	56639		
B0809+74	1.2922	5.733(1)	49162	5.771(2)	56285	5.755(3)	55480
B0818-13	1.2381	40.938(3)	48904	40.981(2)	56568		
B0823+26	0.5307	19.454(4)	46450	19.4789(2)	56665	19.484(6)	55480
B0834+06	1.2738	12.889(6)	48721	12.8640(4)	56864	12.872(4)	55480
B0906-17	0.4016	15.888(3)	48737	15.879(2)	56980		
B0919+06	0.4306	27.271(6)	55140	27.2986(5)	56285	27.316(6)	55480
B0943+10	1.0977	15.4(5)	48483	15.334(1)	56365	15.339(4)	55480
B0950+08	0.2531	2.958(3)	46375	2.96927(8)	56285	2.972(2)	55480
B1112+50	1.6564	9.195(8)	49334	9.1830(4)	56687	9.185(4)	55480
B1133+16	1.1879	4.8451(1)	46407	4.8480(2)	56743	4.846(2)	55480
B1237+25	1.3824	9.242(6)	46531	9.2575(3)	56864	9.268(2)	55480
B1508+55	0.7397	19.613(20)	49904	19.6191(3)	56284	19.622(9)	55480
B1540-06	0.7091	18.403(4)	49423	18.3774(9)	56842	18.334(100)	55480
B1541+09	0.7484	35.24(3)	48716	35.012(5)	56842		
B1604-00	0.4218	10.682(5)	46973	10.6823(1)	56843	10.688(2)	55480
B1612+07	1.2068	21.39(3)	49897	21.3949(3)	56843	21.402(14)	55480
B1642-03	0.3877	35.727(3)	46515	35.7555(8)	56842		
B1706-16	0.6531	24.873(5)	46993	24.891(1)	56843		
B1749-28	0.5626	50.372(8)	46483	50.39(1)	56568		
B1822-09	0.7690	19.38(4)	54262	19.3833(9)	56843	19.408(21)	55480
B1839+56	1.6529	26.698(11)	48717	26.774(1)	56843	26.804(6)	55480
B1842+14	0.3755	41.510(4)	49362	41.498(1)	56860		
B1919+21	1.3373	12.4370(1)	48999	12.4386(3)	56830	12.435(4)	55480
B1929+10	0.2265	3.180(4)	46523	3.1828(5)	56294	3.180(2)	55480
B2016+28	0.5580	14.172(4)	46384	14.1977(6)	57009	14.200(7)	55480
B2020+28	0.3434	24.640(3)	49692	24.632(1)	56567		
B2110+27	1.2029	25.113(4)	48741	25.1171(2)	56842	25.114(18)	55480
J2145-0750	0.0161	8.9977(14)	53040	9.00470(9)	56403		
B2217+47	0.5385	43.519(12)	46599	43.4975(5)	56842		
B2303+30	1.5759	49.544(16)	48714	49.639(6)	57048		
B2327-20	1.6436	8.458(13)	49878	8.456(2)	56979		

Table 2
Dispersion Measures for 44 pulsars detected by LWA1. We also list the DM values reported in the ATNF catalog as well as values reported in (Zakharenko et al. 2013)

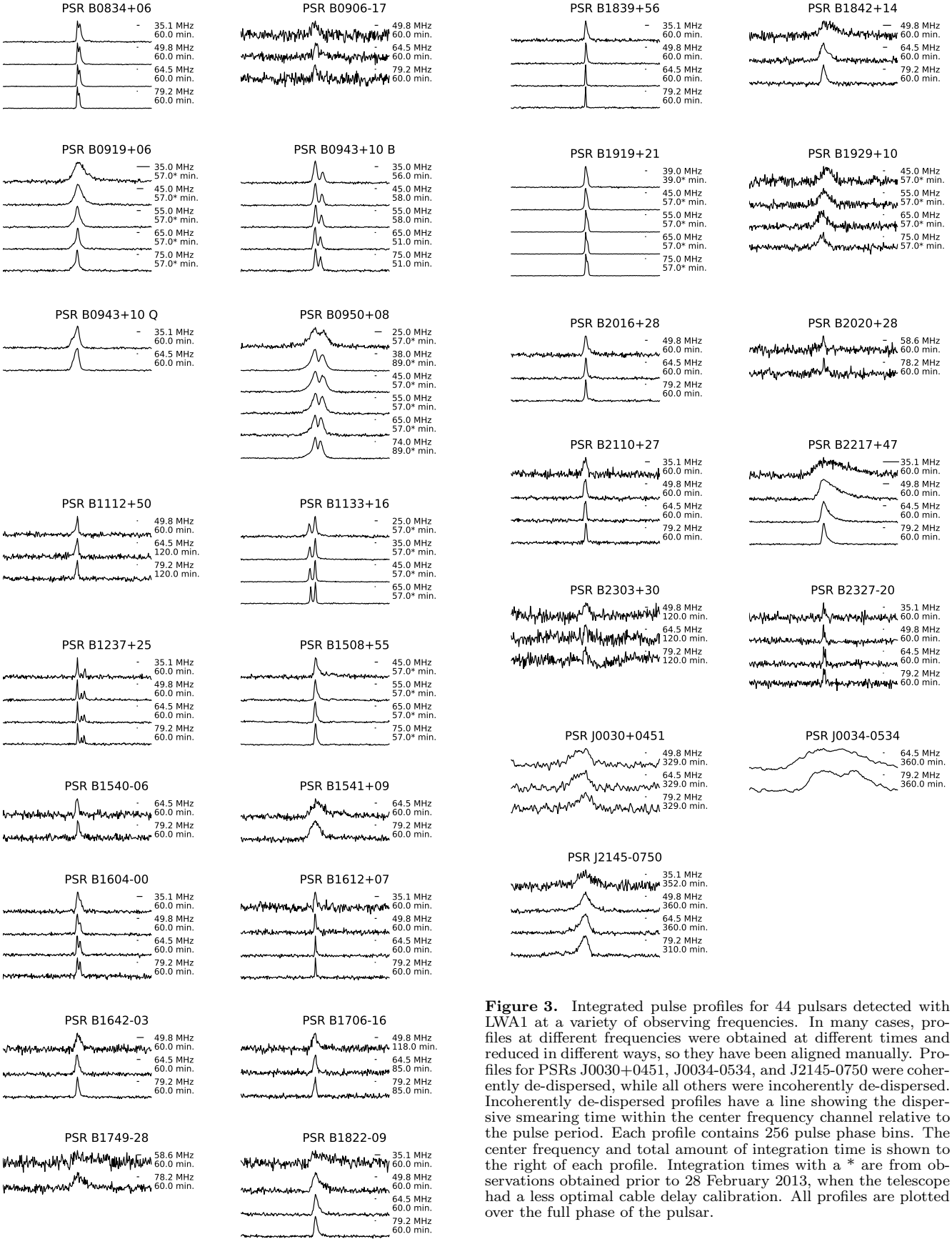

Figure 3. Integrated pulse profiles for 44 pulsars detected with LWA1 at a variety of observing frequencies. In many cases, profiles at different frequencies were obtained at different times and reduced in different ways, so they have been aligned manually. Profiles for PSRs J0030+0451, J0034-0534, and J2145-0750 were coherently de-dispersed, while all others were incoherently de-dispersed. Incoherently de-dispersed profiles have a line showing the dispersive smearing time within the center frequency channel relative to the pulse period. Each profile contains 256 pulse phase bins. The center frequency and total amount of integration time is shown to the right of each profile. Integration times with a * are from observations obtained prior to 28 February 2013, when the telescope had a less optimal cable delay calibration. All profiles are plotted over the full phase of the pulsar.

Pulsar	ν MHz	T min.	w_{50} phase	w_{10} phase	SNR	SEFD kJy	S_ν mJy	α
B0031-07	35.1	60	0.074	0.242	196.29	14.88	3490(1740)	0.5(2)
B0031-07	49.8	60	0.137	0.246	318.75	11.91	6370(3190)	
B0031-07	64.5	60	0.160	0.223	331.25	11.91	7260(3630)	
B0031-07	79.2	60	0.121	0.188	271.99	11.91	5070(2540)	
B0138+59	58.6	60	0.027	0.051	73.65	8.89	460(230)	
B0138+59	78.2	60	0.020	0.043	80.22	8.89	420(210)	
B0149-16	35.1	60	0.027	0.047	59.76	18.85	800(400)	-1.6(1)
B0149-16	49.8	60	0.012	0.043	82.86	15.09	570(290)	
B0149-16	64.5	60	0.012	0.027	69.72	15.09	480(240)	
B0149-16	79.2	60	0.004	0.031	49.54	15.09	200(100)	
B0301+19	64.5	120	0.023	0.039	35.85	7.47	120(60)	
B0301+19	79.2	120	0.020	0.043	42.64	7.47	130(70)	
B0320+39	39.0	60	0.020	0.062	43.51	8.37	220(110)	
B0320+39	58.6	60	0.020	0.035	58.28	6.70	230(120)	
B0329+54	35.1	29	0.070	0.191	186.06	10.94	3370(1680)	0.00(9)
B0329+54	45.0	60	0.066	0.195	422.49	8.15	3870(1940)	
B0329+54	49.8	29	0.035	0.129	414.30	8.75	4160(2080)	
B0329+54	55.0	60	0.031	0.102	541.62	8.15	3340(1670)	
B0329+54	65.0	60	0.023	0.078	574.76	8.15	3060(1530)	
B0329+54	74.0	13	0.016	0.051	354.11	10.16	4070(2030)	
B0355+54	79.2	60	0.059	0.113	52.91	8.10	450(230)	
B0450+55	39.0	60	0.059	0.113	64.03	10.34	700(350)	-1.3(2)
B0450+55	58.6	59	0.023	0.117	126.84	8.28	690(350)	
B0450+55	78.2	59	0.020	0.043	56.94	8.28	280(140)	
B0525+21	39.0	60	0.055	0.105	106.63	9.04	980(490)	-0.8(1)
B0525+21	58.6	60	0.027	0.059	109.17	7.24	560(280)	
B0525+21	78.2	60	0.023	0.039	123.62	7.24	580(290)	
B0628-28	35.1	60	0.082	0.152	125.32	28.71	4540(2270)	0.40(3)
B0628-28	49.8	60	0.074	0.137	193.16	22.97	5300(2650)	
B0628-28	64.5	60	0.059	0.113	223.86	22.97	5410(2710)	
B0628-28	79.2	60	0.059	0.113	271.47	22.97	6560(3280)	
B0655+64	49.8	49	0.043	0.082	67.75	9.52	640(320)	-0.7(1)
B0655+64	64.5	49	0.039	0.055	70.96	9.52	640(320)	
B0655+64	79.2	49	0.035	0.059	53.58	9.52	460(230)	
B0818-13	58.6	60	0.020	0.043	44.50	14.04	370(190)	
B0818-13	78.2	60	0.020	0.035	71.46	14.04	600(300)	
B0823+26	64.5	119	0.020	0.043	111.52	6.84	450(230)	
B0823+26	79.2	119	0.020	0.035	17.16	6.84	70(30)	
B0834+06	35.1	60	0.027	0.051	345.45	11.44	2790(1400)	0.5(1)
B0834+06	49.8	60	0.027	0.047	723.39	9.16	4680(2340)	
B0834+06	64.5	60	0.023	0.039	800.31	9.16	4790(2390)	
B0834+06	79.2	60	0.023	0.031	667.24	9.16	3990(2000)	
B0906-17	49.8	60	0.051	0.090	47.71	15.61	730(360)	-1.65(1)
B0906-17	64.5	60	0.027	0.051	42.61	15.61	470(240)	
B0906-17	79.2	60	0.027	0.051	30.45	15.61	340(170)	
B1112+50	35.1	60	0.020	0.027	27.34	7.66	120(60)	0.7(2)
B1112+50	49.8	60	0.016	0.051	76.58	7.66	310(160)	
B1112+50	64.5	60	0.020	0.035	55.09	7.66	250(130)	
B1112+50	79.2	60	0.020	0.035	44.34	7.66	200(100)	
B1133+16	35.1	60	0.023	0.066	600.98	9.84	3850(1930)	0.30(5)
B1133+16	45.0	100	0.020	0.059	1024.48	8.55	4040(2020)	
B1133+16	49.8	60	0.020	0.059	1008.95	7.88	4710(2360)	
B1133+16	64.5	60	0.020	0.051	1096.32	7.88	5120(2560)	
B1133+16	79.2	60	0.020	0.047	1012.97	7.88	4730(2370)	
B1237+25	35.1	60	0.012	0.043	69.96	8.73	280(140)	0.0(2)
B1237+25	49.8	60	0.012	0.047	158.29	6.98	510(250)	
B1237+25	64.5	60	0.012	0.039	160.37	6.98	510(260)	
B1237+25	79.2	60	0.004	0.039	141.41	6.98	260(130)	
B1508+55	58.6	14	0.016	0.047	236.95	8.24	2130(1060)	
B1508+55	78.2	14	0.016	0.039	285.24	8.24	2560(1280)	
B1540-06	49.8	60	0.020	0.035	38.91	11.67	270(140)	-1.7(4)
B1540-06	64.5	60	0.020	0.035	46.68	11.67	320(160)	
B1540-06	79.2	60	0.020	0.035	17.18	11.67	120(60)	
B1541+09	64.5	60	0.098	0.184	167.85	8.67	2020(1010)	
B1541+09	79.2	60	0.074	0.129	66.21	8.67	690(340)	
B1604-00	35.1	60	0.035	0.055	153.93	12.66	1570(780)	-1.5(1)
B1604-00	49.8	60	0.023	0.047	181.30	10.13	1200(600)	
B1604-00	64.5	60	0.023	0.043	149.07	10.13	990(490)	
B1604-00	79.2	60	0.020	0.039	75.03	10.13	450(230)	
B1612+07	35.1	60	0.020	0.027	30.53	11.16	200(100)	-0.72(6)
B1612+07	49.8	60	0.012	0.020	43.17	8.93	180(90)	
B1612+07	64.5	60	0.004	0.023	64.70	8.93	150(80)	
B1612+07	79.2	60	0.004	0.012	44.82	8.93	110(50)	
B1642-03	49.8	60	0.043	0.074	78.63	10.93	770(380)	0.2(1)
B1642-03	64.5	60	0.027	0.051	120.04	10.93	930(460)	
B1642-03	79.2	60	0.020	0.035	126.84	10.93	830(410)	
B1706-16	49.8	60	0.035	0.059	73.83	15.15	900(450)	-0.65(5)
B1706-16	64.5	60	0.020	0.043	79.31	15.15	710(360)	
B1706-16	79.2	60	0.020	0.035	74.02	15.15	670(330)	
B1749-28	78.2	60	0.082	0.152	117.02	22.57	3330(1660)	
B1822-09	35.1	60	0.160	0.293	106.51	15.70	3080(1540)	-0.77(2)

Pulsar	ν MHz	T min.	w_{50} phase	w_{10} phase	SNR	SEFD kJy	S_ν mJy	α
B1822-09	49.8	60	0.047	0.141	189.29	12.56	2220(1110)	
B1822-09	64.5	60	0.027	0.070	209.32	12.56	1860(930)	
B1822-09	79.2	60	0.023	0.059	200.24	12.56	1640(820)	
B1839+56	35.1	60	0.020	0.047	136.16	10.50	850(430)	-1.7(2)
B1839+56	49.8	60	0.012	0.027	176.24	8.40	680(340)	
B1839+56	64.5	60	0.012	0.012	135.70	8.40	520(260)	
B1839+56	79.2	60	0.004	0.012	94.31	8.40	210(100)	
B1842+14	49.8	60	0.129	0.230	159.79	7.97	2070(1030)	-2.8(3)
B1842+14	64.5	60	0.047	0.117	178.22	7.97	1330(660)	
B1842+14	79.2	60	0.035	0.059	127.88	7.97	820(410)	
B1919+21	35.1	358	0.020	0.055	738.05	9.05	1620(810)	0.17(2)
B1919+21	49.8	358	0.020	0.043	922.67	7.24	1630(810)	
B1919+21	64.5	358	0.020	0.035	979.29	7.24	1730(860)	
B1919+21	79.2	358	0.020	0.031	1055.24	7.24	1860(930)	
B2016+28	49.8	60	0.023	0.078	135.41	6.66	590(290)	-0.18(9)
B2016+28	64.5	60	0.020	0.035	127.30	6.66	500(250)	
B2016+28	79.2	60	0.012	0.039	178.14	6.66	550(270)	
B2020+28	58.6	60	0.020	0.035	28.37	6.65	110(60)	
B2020+28	78.2	60	0.012	0.020	19.26	6.65	60(30)	
B2110+27	35.1	60	0.035	0.059	60.18	8.44	410(200)	-0.5(1)
B2110+27	49.8	60	0.020	0.043	111.89	6.75	450(220)	
B2110+27	64.5	60	0.020	0.027	99.09	6.75	400(200)	
B2110+27	79.2	60	0.012	0.027	86.06	6.75	270(130)	
B2217+47	35.1	60	0.250	0.492	470.76	9.79	11220(5610)	-1.8(2)
B2217+47	49.8	60	0.121	0.316	823.71	7.83	10100(5050)	
B2217+47	64.5	60	0.051	0.156	732.30	7.83	5600(2800)	
B2217+47	79.2	60	0.023	0.082	492.77	7.83	2520(1260)	
B2303+30	49.8	120	0.043	0.074	42.24	6.65	180(90)	-3.3(6)
B2303+30	64.5	120	0.020	0.035	19.24	6.65	50(30)	
B2303+30	79.2	120	0.020	0.035	18.44	6.65	50(30)	
B2327-20	35.1	60	0.020	0.035	25.98	20.93	320(160)	-0.5(1)
B2327-20	49.8	60	0.004	0.004	69.63	16.75	310(150)	
B2327-20	64.5	60	0.004	0.016	46.02	16.75	200(100)	
B2327-20	79.2	60	0.016	0.020	27.87	16.75	250(120)	

Table 3 Mean flux density (S_ν) measurements for 36 pulsars detected using LWA1 at multiple observing frequencies (ν and measured spectral indices for pulsars with more than 2 measurements of S_ν. We also give the integration time (T) of the observations used in these measurements as well as pulse width at half-maximum (w_{50}) and 10% of maximum (w_{10}).

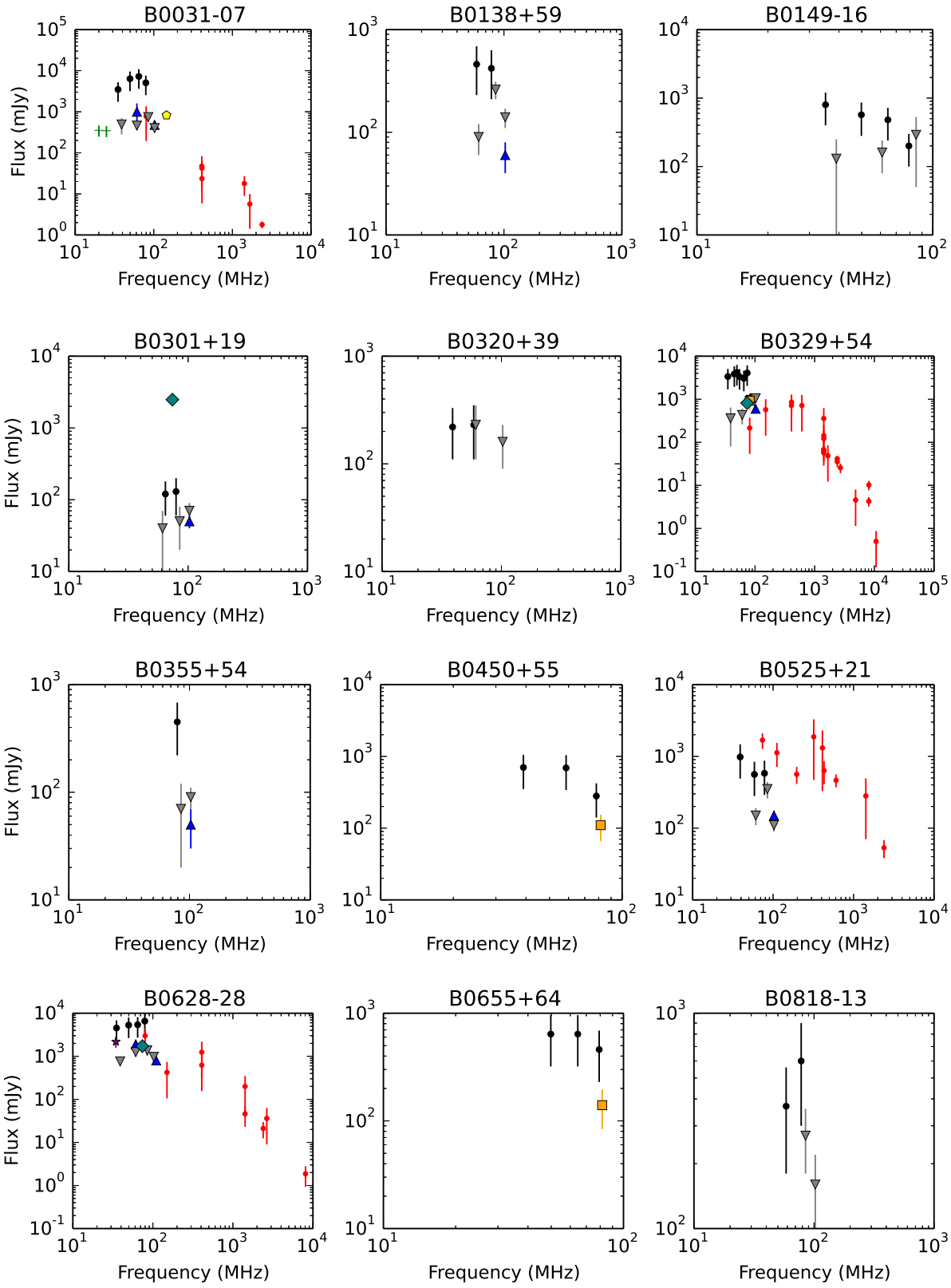
B0031-07
B0138+59
B0149-16
B0301+19
B0320+39
B0329+54
B0355+54
B0450+55
B0525+21
B0628-28
B0655+64
B0818-13
Flux (mJy)
Frequency (MHz)

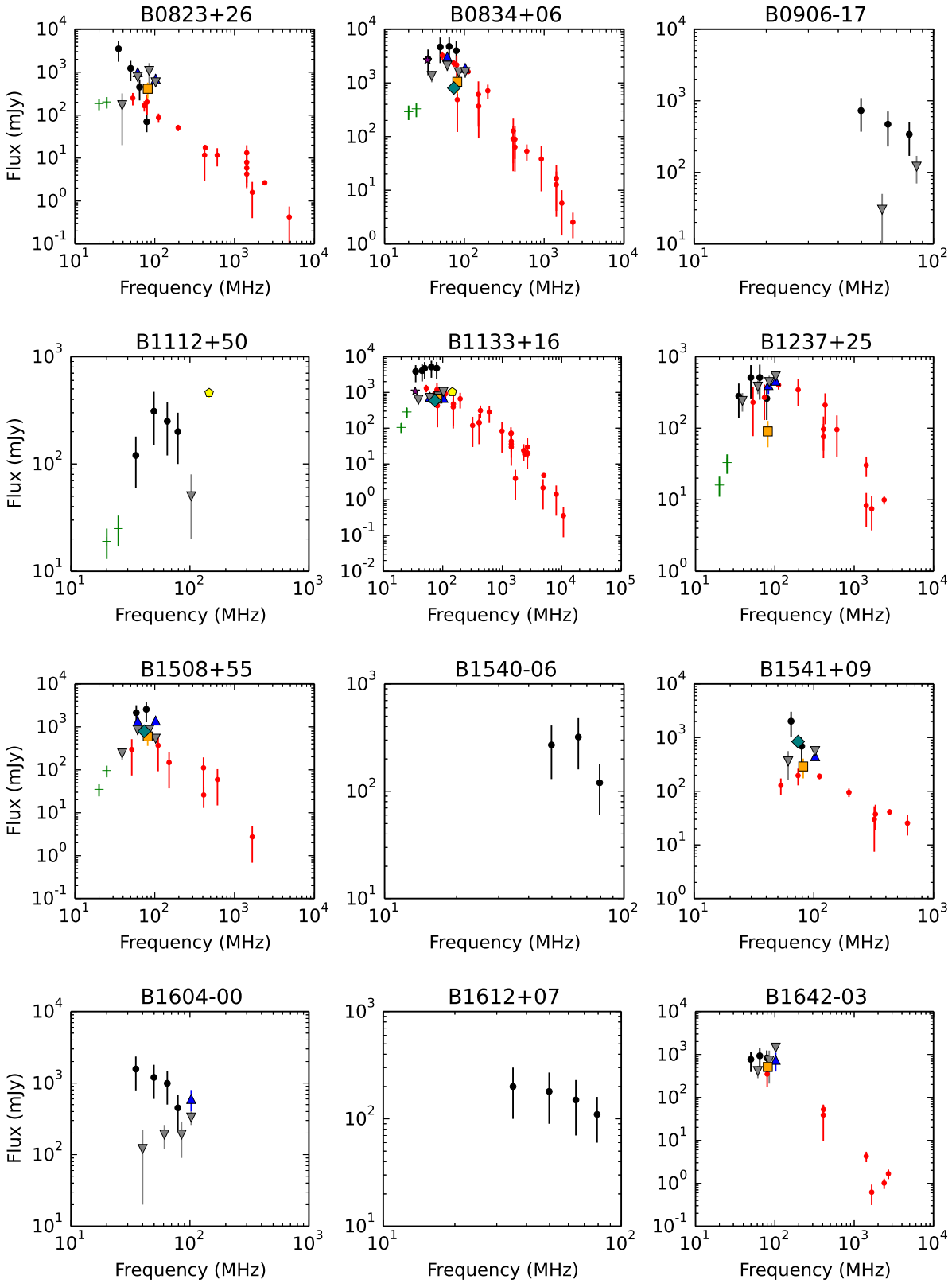
B0823+26
B0834+06
B0906-17
B1112+50
B1133+16
B1237+25
B1508+55
B1540-06
B1541+09
B1604-00
B1612+07
B1642-03
Flux (mJy)
Frequency (MHz)

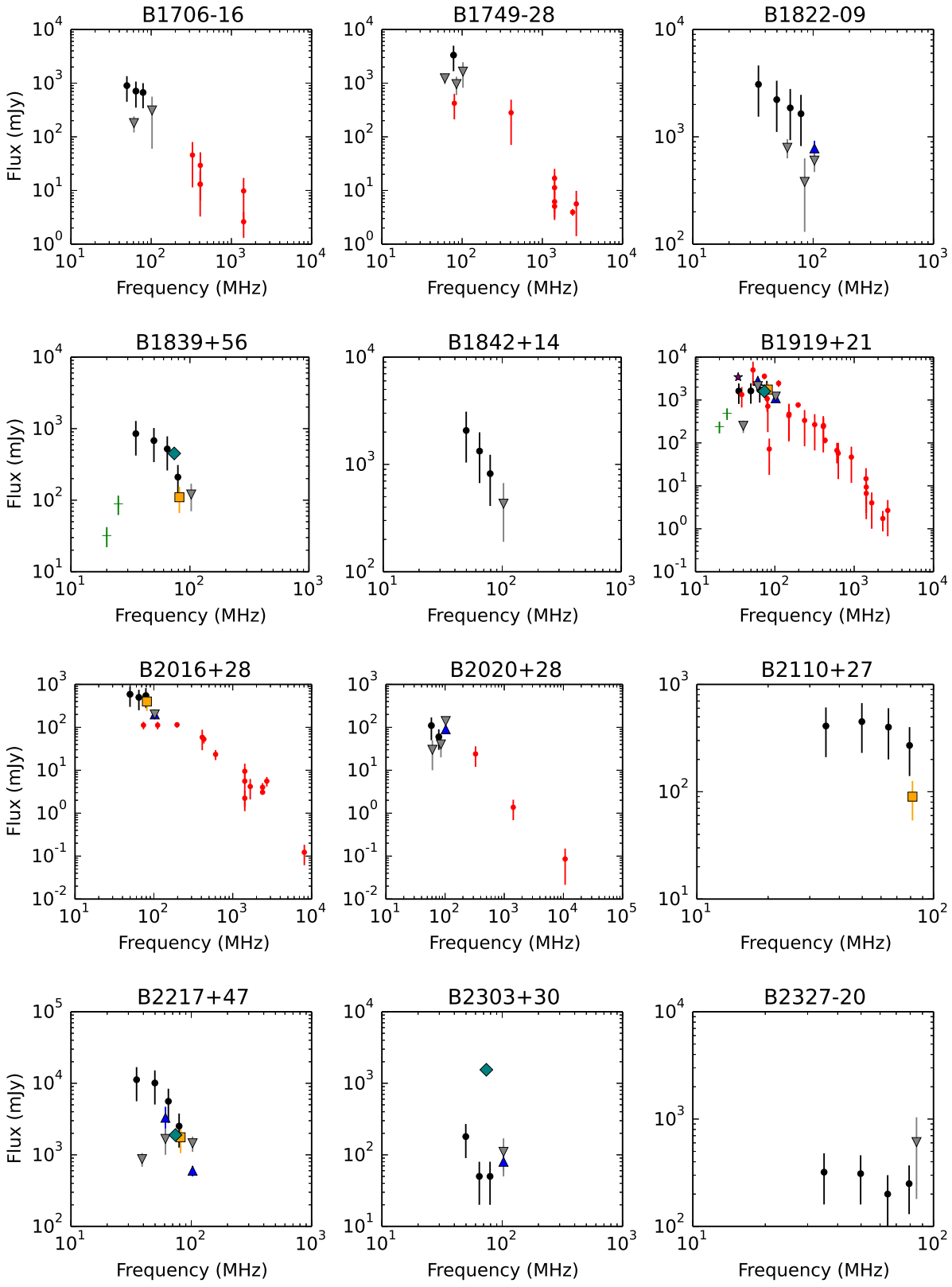

Figure 4. Flux density measurements for 36 pulsars at a variety of frequencies obtained using LWA1 plotted are plotted with values at comparable frequencies. Black filled circles are our measurements, red filled circles are from Sieber (1973), blue up triangles are from Izvekova et al. (1979), gray down trianges are from Izvekova et al. (1981), purple stars are from Deshpande & Radhakrishnan (1992), orange squares are from Shrauner et al. (1998), yellow pentagons are from Karuppusamy et al. (2011), green pluses are from Zakharenko et al. (2013), and teal diamonds are from Lane et al. (2014).

For 27 of the pulsars, we measured mean flux densities at three or more frequencies and performed a linear fit for a spectral index across all or a portion of the LWA1 band. The spectral indices that we determined are given in Table 3 and Figure 5 shows a histogram of these values. The distribution of spectral indices has a mean of −0.7 and a standard deviation of 1.0. A comparison of the mean of this low frequency distribution to the mean (−1.41) of Bates et al. (2013) which was derived based on pulsar observations near 1 GHz provides further evidence for turnover in pulsar spectra near 100 MHz.

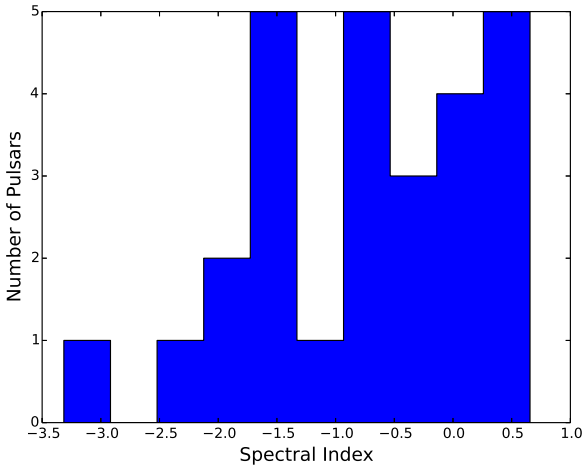

Figure 5. The distribution of spectral indices in the frequency range 30 to 88 MHz for 27 pulsars.

6.3. *Pulse Component Analysis*

In Tables 4 and 5, we present separation of components and individual component widths for 2 and 3 component profiles, respectively. Ten of the detected profiles required 2 Gaussian components while five required 3 Gaussian components. PSR B0943+10 is included in both tables because in B mode, it has 3 components while in Q mode, only 2 components were required during profile fitting. Combining the analysis of these individual components with the overall profiles widths, w_{50} and w_{10}, shows a general trend for these parameters to increase with decreasing frequencies, supporting RFM. However, there are some exceptions, such as PSR B1919+21 which does not show any increase in any of these parameters, but rather a decrease (with the exception of w_{10}) as frequency decreases. This has been previously observed for PSR B1919+21 (e.g. Mitra & Rankin 2002). Other exceptions include PSRs B0149−16 and B1112+50. Though the overall width of PSR B0149−16 increases at lower frequency, the separation of its two components remains constant. The overall increase is due to the increase in width of the components. In the single component PSR B1112+50, both w_{50} and w_{10} are unchanged over the LWA1 frequency band.

In addition to evolution of the width of pulsar profiles as well as individual components, considerable change in the relative amplitudes of individual components. In Table 4, we compare the relative amplitudes of the 2 components at various frequencies. PSRs B0031-07, B0809+74, and B1919+21 all show considerable changes within the LWA1 observing band. Others, including B0149-16, B0301+19 and B2327-20 seem to have a slight trend in profile evolution, while the other 4 pulsars listed are relatively unchanged in the LWA1 band or have too few measurements reported here.

Pulsar	ν MHz	$\Delta\phi_{12}$ phase	w_{50}^1 phase	w_{50}^2 phase	A_{21}
B0031-07	35.1	0.111(7)	0.08(1)	0.070(5)	2.2(5)
	49.8	0.10(1)	0.11(2)	0.068(5)	1.4(2)
	64.5	0.085(6)	0.079(8)	0.063(6)	1.3(2)
	79.2	0.07(1)	0.047(7)	0.09(1)	1.3(3)
B0149-16	35.1	0.021(2)	0.012(1)	0.017(2)	1.0(2)
	49.8	0.021(1)	0.0094(6)	0.018(2)	0.8(1)
	64.5	0.0222(9)	0.0082(5)	0.013(2)	0.6(1)
	79.2	0.020(1)	0.0071(6)	0.016(3)	0.7(2)
B0301+19	49.8	0.062(4)	0.030(6)	0.027(4)	1.2(4)
	64.5	0.058(2)	0.013(2)	0.011(2)	0.9(3)
	79.2	0.053(2)	0.014(2)	0.008(2)	0.6(2)
B0320+39	39.0	0.030(3)	0.017(3)	0.019(5)	0.6(2)
	58.6	0.017(1)	0.013(1)	0.011(2)	0.6(1)
	78.2	0.016(1)	0.013(1)	0.013(2)	0.9(2)
B0525+21	39.0	0.063(2)	0.030(3)	0.029(3)	0.9(1)
	58.6	0.0601(8)	0.0153(7)	0.019(1)	0.88(8)
	68.0	0.054(2)	0.012(1)	0.012(2)	0.6(2)
	78.2	0.0555(5)	0.0107(5)	0.0115(6)	0.87(7)
B0809+74	35.0	0.077(5)	0.069(9)	0.056(3)	1.8(3)
	45.0	0.068(4)	0.048(5)	0.054(4)	1.7(3)
	55.0	0.055(2)	0.036(1)	0.060(2)	2.0(2)
	75.0	0.027(2)	0.026(2)	0.066(1)	4.8(8)
B0943+10Q	35.1	0.035(2)	0.032(3)	0.032(1)	2.4(4)
	64.5	0.026(3)	0.029(3)	0.031(1)	3.2(9)
B1604-00	35.1	0.019(8)	0.017(3)	0.028(9)	1.0(9)
	49.8	0.019(1)	0.0142(7)	0.017(1)	0.7(1)
	64.5	0.0192(6)	0.0101(5)	0.016(1)	1.0(1)
	79.2	0.0180(9)	0.011(1)	0.011(1)	0.9(1)
B1919+21	55.0	0.0075(1)	0.0061(1)	0.0213(1)	4.1(1)
	65.0	0.0081(1)	0.00630(8)	0.0201(1)	3.5(1)
	75.0	0.0113(2)	0.0085(1)	0.0133(2)	1.12(4)
B2327-20	35.1	0.012(2)	0.010(2)	0.006(1)	0.5(2)
	49.8	0.010(2)	0.006(2)	0.009(4)	0.6(3)
	64.5	0.0105(7)	0.0061(8)	0.0064(8)	0.9(2)
	79.2	0.009(1)	0.007(2)	0.006(1)	1.0(4)

Table 4 Component spacing and widths for 10 pulsars with two components in the LWA1 frequency band.

Pulsar	ν MHz	$\Delta\phi_{13}$ phase	$\Delta\phi_{12}$ phase	$\Delta\phi_{23}$ phase	w_{50}^1 phase	w_{50}^2 phase	w_{50}^3 phase
B0834+06	35.1	0.039(4)	0.0156(4)	0.024(4)	0.0090(3)	0.0218(7)	0.084(7)
	49.8	0.020(1)	0.0140(2)	0.006(1)	0.0086(2)	0.0132(4)	0.034(1)
	64.5	0.019(1)	0.0127(1)	0.006(1)	0.0080(1)	0.0121(3)	0.031(1)
	79.2	0.020(4)	0.0120(1)	0.008(4)	0.0078(1)	0.0120(3)	0.030(4)
B0943+10B	35.0	0.0501(6)	0.013(9)	0.037(9)	0.0254(8)	0.13(2)	0.024(1)
	45.0	0.0459(5)	0.014(5)	0.031(5)	0.0214(5)	0.08(1)	0.0210(9)
	55.0	0.0396(5)	0.017(4)	0.023(4)	0.0194(5)	0.074(8)	0.020(1)
	65.0	0.0369(4)	0.022(4)	0.015(4)	0.0180(5)	0.077(9)	0.0178(9)
	75.0	0.0334(5)	0.015(4)	0.019(4)	0.0169(7)	0.08(1)	0.018(1)
B0950+08	25.0	0.065(4)	0.015(7)	0.050(7)	0.050(6)	0.19(2)	0.048(5)
	38.0	0.055(1)	-0.024(8)	0.079(8)	0.032(2)	0.081(8)	0.047(1)
	45.0	0.054(2)	-0.02(1)	0.08(1)	0.031(3)	0.07(1)	0.050(2)
	55.0	0.0512(9)	0.007(3)	0.045(3)	0.031(2)	0.130(5)	0.030(1)
	65.0	0.043(2)	-0.02(1)	0.07(1)	0.025(2)	0.07(1)	0.037(2)
	74.0	0.0396(3)	0.003(1)	0.037(1)	0.0214(5)	0.109(2)	0.0253(6)
B1133+16	35.1	0.0357(1)	0.0259(9)	0.0099(9)	0.0127(3)	0.063(2)	0.0124(2)
	49.8	0.03317(7)	0.0188(7)	0.0143(6)	0.0113(1)	0.060(1)	0.01138(7)
	64.5	0.03101(5)	0.0151(7)	0.0159(7)	0.00943(8)	0.047(1)	0.01041(6)
	79.2	0.02917(5)	0.0135(7)	0.0157(7)	0.00857(8)	0.0412(9)	0.00976(7)
B1237+25	35.1	0.0496(9)	0.026(2)	0.024(2)	0.0097(7)	0.009(4)	0.011(1)
	49.8	0.0485(5)	0.0270(5)	0.0215(7)	0.0094(3)	0.0079(8)	0.0127(8)
	64.5	0.0455(4)	0.0261(4)	0.0193(6)	0.0084(2)	0.0088(8)	0.0109(7)
	79.2	0.0438(3)	0.0249(6)	0.0189(7)	0.0074(2)	0.012(1)	0.0087(6)

Table 5 Component spacing and widths for 5 pulsars with 3 components in the LWA1 frequency range.

7. CONCLUSION

We have presented detections of 44 pulsars using LWA1, including precise DM measurements for all 44 and mean flux density measurements at a variety of frequencies within 40–88 MHz for 36 of them. As expected, our flux density measurements confirm spectral turnover in many of the pulsars we have detected. The mean flux density measurements presented in this paper did not account for the effect of LST on the LWA1 SEFD and therefore have larger errors than we believe to be possible in the near future. We intend to enhance our SEFD model for LWA1, enabling much more precise measurements of pulsar flux densities, which will allow improved studies of the spectral properties of pulsars. We have also presented component spacing and widths for 15 profiles (14 pulsars since B0943+10 has two modes) which required either 2 or 3 components to adequately model the profile. For 2-component profiles, we have also compared the ratio of the second peak to that of the first. These detections demonstrate the capabilities of LWA1 for use in pulsar astronomy work, including the detection of 3 MSPs to date, J0030+0451, J0034-0534, and J2145-0750. LWA1's observing band goes down to the lowest frequencies observable through the Earth's ionosphere. Observations at these frequencies are very important for understanding the ISM as well as the pulsars themselves. A comparison of our measured DMs to those reported in previous work show that the DM has changed significantly since the original measurement. The derived rate of change is comparable to past DM variation measurements, however these changes can easily be monitored using LWA1. Further work needs to be done to account for possible bias in the DM measurements due to profile evolution, however the observed difference in DM is too large to be due to profile evolution alone. The observations presented here resulted in DM measurements with errors of order 10^{-5}pc cm^{-3}, in some pulsars. Periodic measurements with this precision of many pulsars will enhance our understanding of the ISM and may enable improved correction for DM variation of data sets used in attempts to detect the signal of GWs using PTAs. We have begun monitoring the 3 MSPs for DM variation over time and based on the results presented above, we will also monitor pulsars that have shown significant changes and present those results in future publications. We have also presented profiles for 44 pulsars, some of which show considerable profile evolution over the LWA1 frequency band. Some of the profile evolution is likely due to interstellar scattering which will be investigated further and presented in future work. Profile evolution seen in PSRs B0031-07, B0320+39, and B0809+74 consists of considerable change in the ratio of the amplitude of the 2 components making up their profiles. An analysis of component width and spacing largely supports RFM throughout the LWA1 band, however there are a few exceptions. We have also introduced the open access LWA Pulsar Data Archive, where we are archiving pulsar observations performed with LWA1 in a variety of reduced data formats suitable for analysis of folded pulsar data as well as single pulse analysis.

ACKNOWLEDGEMENTS

Construction of the LWA has been supported by the Office of Naval Research under Contract N00014-07-C-0147. Support for operations and continuing development of the LWA1 is provided by the National Science Foundation under grants AST-1139963 and AST-1139974 of the University Radio Observatory program. Basic research on pulsars at NRL is supported by the Chief of Naval Research (CNR). Part of this research was carried out at the Jet Propulsion Laboratory, California Institute of Technology, under a contract with the National Aeronautics and Space Administration. The authors thank an anonymous referee for their useful comments.

Facilities: LWA

REFERENCES

Ahuja, A. L., Mitra, D., & Gupta, Y. 2007, MNRAS, 377, 677
Bates, S. D., Lorimer, D. R., & Verbiest, J. P. W. 2013, MNRAS, 431, 1352

Bhat, N. D. R., Ord, S. M., Tremblay, S. E., et al. 2014, ApJ, 791, L32
Bilous, A. V., Hessels, J. W. T., Kondratiev, V. I., et al. 2014, A&A, 572, A52
Braude, S. I., Megn, A. V., Riabov, B. P., Sharykin, N. K., & Zhuk, I. N. 1978, Ap&SS, 54, 3
Cordes, J. M. 1978, ApJ, 222, 1006
Cordes, J. M. 2002, in Astronomical Society of the Pacific Conference Series, Vol. 278, Single-Dish Radio Astronomy: Techniques and Applications, ed. S. Stanimirovic, D. Altschuler, P. Goldsmith, & C. Salter, 227
Cordes, J. M., & Shannon, R. M. 2010, ArXiv e-prints, arXiv:1010.3785 [astro-ph.IM]
Cordes, J. M., Shannon, R. M., & Stinebring, D. R. 2015, ArXiv e-prints, arXiv:1503.08491 [astro-ph.IM]
Dembska, M., Kijak, J., Jessner, A., et al. 2014, MNRAS, 445, 3105
Demorest, P. B., Ferdman, R. D., Gonzalez, M. E., et al. 2013, ApJ, 762, 94
Demorest, P. B. e. a. 2015, in prep.
Deshpande, A. A., & Radhakrishnan, V. 1992, Journal of Astrophysics and Astronomy, 13, 151
Desvignes, G., e. a. 2015, in prep.
Dewey, R. J., Taylor, J. H., Weisberg, J. M., & Stokes, G. H. 1985, ApJ, 294, L25
Dowell, J., Wood, D., Stovall, K., et al. 2012, Journal of Astronomical Instrumentation, 1, 50006
Dowell, J., Ray, P. S., Taylor, G. B., et al. 2013, ApJ, 775, L28
Ellingson, S. W., Clarke, T. E., Craig, J., et al. 2013a, ApJ, 768, 136
Ellingson, S. W., Taylor, G. B., Craig, J., et al. 2013b, IEEE Transactions on Antennas and Propagation, 61, 2540
Frigo, M., & Johnson, S. G. 1998, in (IEEE), 1381
Haslam, C. G. T., Salter, C. J., Stoffel, H., & Wilson, W. E. 1982, A&AS, 47, 1
Hassall, T. E., Stappers, B. W., Hessels, J. W. T., et al. 2012, A&A, 543, A66
Hewish, A., Bell, S. J., Pilkington, J. D. H., Scott, P. F., & Collins, R. A. 1968, Nature, 217, 709
Hotan, A. W., van Straten, W., & Manchester, R. N. 2004, PASA, 21, 302
Izvekova, V. A., Kuzmin, A. D., Malofeev, V. M., & Shitov, I. P. 1981, Ap&SS, 78, 45
Izvekova, V. A., Kuz'min, A. D., Malofeev, V. M., & Shitov, Y. P. 1979, Soviet Ast., 23, 179
Karastergiou, A., & Johnston, S. 2007, MNRAS, 380, 1678
Karuppusamy, R., Stappers, B. W., & Serylak, M. 2011, A&A, 525, A55
Kijak, J., Gupta, Y., & Krzeszowski, K. 2007, A&A, 462, 699
Lane, W. M., Cotton, W. D., van Velzen, S., et al. 2014, MNRAS, 440, 327
Löhmer, O., Kramer, M., Mitra, D., Lorimer, D. R., & Lyne, A. G. 2001, ApJ, 562, L157
Lyne, A. G., & Manchester, R. N. 1988, MNRAS, 234, 477
Malofeev, V. M., Gil, J. A., Jessner, A., et al. 1994, A&A, 285, 201
Manchester, R. N., Hobbs, G., Bailes, M., et al. 2012, ArXiv e-prints, arXiv:1210.6130 [astro-ph.IM]
Mitra, D., & Rankin, J. M. 2002, ApJ, 577, 322
Phillips, J. A. 1991, ApJ, 373, L63
Phillips, J. A., & Wolszczan, A. 1991, ApJ, 382, L27
Pilia, M., Hessels, J. W. T., Stappers, B. W., et al. 2015, A & A, submitted
Rankin, J. M. 1983, ApJ, 274, 333
Ransom, S. M. 2001, PhD thesis, Harvard University
Ryabov, V. B., Vavriv, D. M., Zarka, P., et al. 2010, A&A, 510, A16
Schinzel, F., & Dowell, J. 2014, LWA Memo Series
Schinzel, F., & Polisensky, E. 2014, LWA Memo Series
Shrauner, J. A., Taylor, J. H., & Woan, G. 1998, ApJ, 509, 785
Sieber, W. 1973, A&A, 28, 237
Stappers, B. W., Hessels, J. W. T., Alexov, A., et al. 2011, A&A, 530, A80
Suleymanova, S. A., & Izvekova, V. A. 1984, Sov. Astron., 28, 53
Taylor, G. B., Ellingson, S. W., Kassim, N. E., et al. 2012, Journal of Astronomical Instrumentation, 1, 50004
Taylor, J. H. 1992, Philosophical Transactions of the Royal Society of London, 341, 117-134 (1992), 341, 117
Thorsett, S. E. 1991, ApJ, 377, 263
Tingay, S. J., Goeke, R., Bowman, J. D., et al. 2013, PASA, 30, 7
Tremblay, S. E., Ord, S. M., Bhat, N. D. R., et al. 2015, PASA, 32, 5
Tsai, J.-W., Simonetti, J. H., Akukwe, B., et al. 2015, AJ, 149, 65
van Haarlem, M. P., Wise, M. W., Gunst, A. W., et al. 2013, A&A, 556, A2
van Haasteren, R., Levin, Y., Janssen, G. H., et al. 2011, MNRAS, 414, 3117
Zakharenko, V. V., Vasylieva, I. Y., Konovalenko, A. A., et al. 2013, MNRAS, 431, 3624